ARTICLE





Impacts of hydrodynamic conditions and microscale surface roughness on the critical shear stress to develop and thickness of early-stage *Pseudomonas putida* biofilms

Correspondence

Judy Q. Yang, Saint Anthony Falls Laboratory, University of Minnesota, Minneapolis, MN 55414. USA.

Email: judyyang@umn.edu

Funding information

National Science Foundation; Minnesota's Discovery, Research, and Innovation Economy (MnDRIVE) at the University of Minnesota.

Abstract

Biofilms can increase pathogenic contamination of drinking water, cause biofilmrelated diseases, alter the sediment erosion rate, and degrade contaminants in wastewater. Compared with mature biofilms, biofilms in the early-stage have been shown to be more susceptible to antimicrobials and easier to remove. Mechanistic understanding of physical factors controlling early-stage biofilm growth is critical to predict and control biofilm development, yet such understanding is currently incomplete. Here, we reveal the impacts of hydrodynamic conditions and microscale surface roughness on the development of early-stage Pseudomonas putida biofilm through a combination of microfluidic experiments, numerical simulations, and fluid mechanics theories. We demonstrate that early-stage biofilm growth is suppressed under high flow conditions and that the local velocity for early-stage P. putida biofilms (growth time < 14 h) to develop is about 50 µm/s, which is similar to P. putida's swimming speed. We further illustrate that microscale surface roughness promotes the growth of early-stage biofilms by increasing the area of the low-flow region. Furthermore, we show that the critical average shear stress, above which early-stage biofilms cease to form, is 0.9 Pa for rough surfaces, three times as large as the value for flat or smooth surfaces (0.3 Pa). The important control of flow conditions and microscale surface roughness on early-stage biofilm development, characterized in this study, will facilitate future predictions and managements of early-stage P. putida biofilm development on the surfaces of drinking water pipelines, bioreactors, and sediments in aquatic environments.

KEYWORDS

biofilm thickness, critical shear stress, early-stage biofilms, hydrodynamic conditions, microfluidics, microscale surface roughness

This is an open access article under the terms of the Creative Commons Attribution-NonCommercial License, which permits use, distribution and reproduction in any medium, provided the original work is properly cited and is not used for commercial purposes.

© 2023 The Authors. Biotechnology and Bioengineering published by Wiley Periodicals LLC.

¹Saint Anthony Falls Laboratory, University of Minnesota, Minneapolis, Minnesota, USA

²Department of Civil, Environmental, and Geo-Engineering, University of Minnesota, Minneapolis, Minnesota, USA

1 | INTRODUCTION

Biofilms, consortiums of bacterial cells and extracellular polymeric substances (EPS) attached to substrate surfaces (Donlan, 2001), are ubiquitous in rivers (Cho et al., 2022; Drummond et al., 2015; Risse-Buhl et al., 2017; Tlili et al., 2020), coastal areas (De Carvalho, 2018), human organs (Schulze et al., 2021), and drinking water distribution systems (DWDS) (Shen et al., 2016; Yan et al., 2022). Many biofilms are harmful because they increase the presence of pathogenic bacteria (September et al., 2007; Ximenes et al., 2017), clog medical devices (Donlan, 2001; Drescher et al., 2013; Dressaire & Sauret, 2017), and increase bacterial resistance to bactericides (Ghannoum et al., 2020). Many other biofilms, such as those used in moving-bed biofilm reactors (MBBRs) (Bassin et al., 2012), are beneficial because they remove contaminants and excess nutrients from wastewater (Zhu et al., 2010). Biofilms can form different morphologies, including thin film structures (Coyte et al., 2017), wrinkles (Geisel et al., 2022), ripples (Nguyen et al., 2005), and streamers (Drescher et al., 2013; Parvinzadeh Gashti et al., 2015). Fundamental understanding of biofilm morphology is critical to predict and manipulate the function of biofilms (Recupido et al., 2020; Trejo et al., 2013). In this study, we focus on the thickness of thin-film biofilms grown on the microfluidic sidewalls, as biofilm thickness is a key parameter controlling biofilm functionality including the occurrence of biofilm clogging and the efficiency of biofilm-based wastewater treatment plans (Suarez et al., 2019; Torresi et al., 2016). Another key parameter that controls biofilm functionality is the critical condition above which biofilms cease to develop because it informs strategies to prevent biofilm development (Nejadnik et al., 2008: Thomen et al., 2017).

The formation of biofilms is a complex process that involves many steps. Here, we follow some studies that assume that biofilm development can be simplified as four stages (Abu Bakar et al., 2018; Vasudevan, 2014): (1) the initial reversible attachment of planktonic cells to surfaces: (2) the irreversible attachment of bacteria to the surface through the formation of aggregates by producing EPS, (3) the formation of mature multilayer biofilms; and (4) detachment of biofilms and dispersion of cell aggregates and planktonic cells. Note that biofilm development may involve more processes than the above simplified four stages. For example, between first and second stages, cells can be neither irreversibly attached nor embedded in the EPS matrix (Bester et al., 2013). Biofilms in the first and second stages are often referred to as early-stage biofilms (Armbruster & Parsek, 2018; Fu et al., 2021). Compared with mature biofilms, early-stage biofilms are more susceptible to antimicrobials and environmental changes and thus easier to disrupt (Fu et al., 2021; Gu et al., 2019). Systematic understanding of factors that control development of early-stage biofilms is critical for biofilm management, yet such understanding is

Many studies have investigated the molecular mechanisms and genetic functions of biofilms (Davey & O'Toole, 2000; Hall & Mah, 2017; Mielich Süss & Lopez, 2015), yet the impacts of physical environment on biofilm development are less understood. Here, we

investigate two physical factors that control the development of early-stage biofilms: hydrodynamic conditions and the roughness of the substrate surface. Hydrodynamic conditions and surface roughness have shown to play important roles in early-stage biofilm growth (Cowle et al., 2020; Janjaroen et al., 2013; Krsmanovic et al., 2021; Zhang et al., 2011; Zhang et al., 2022; Zheng et al., 2021), yet, their impacts remain controversial. Under different hydrodynamic conditions, shear force can alter the morphology and wetting properties of biofilms (Recupido et al., 2020), change biofilm metabolic behaviors (Liu & Tay, 2002), and control biofilm structures (Stoodley et al., 1998). Some studies show that high flow velocity or shear favors biofilm growth, increases biofilm thickness, and gives rise to a more elastic and resistant biofilm (Liu et al., 2019; Paquet-Mercier et al., 2016; Paramonova et al., 2009). In contrast, some other studies show that high-flow conditions reduce the thickness of biofilms in bioreactors (Lemos et al., 2015). A recent study further shows that bacterial cells sense shear rate instead of shear stress (Sanfilippo et al., 2019). Systematic investigation is needed to reveal the impacts of hydrodynamic conditions on biofilm development.

In addition to hydrodynamic conditions, the roughness of substrate surfaces plays a critical role in biofilm development because surface roughness can interact with flow and bacterial cells (Chinnaraj et al., 2021; Zheng et al., 2021). Currently, the majority of studies on biofilm development focus on flat surfaces (Drescher et al., 2013; Sanfilippo et al., 2019) and surface roughness below 500 nm (Bollen et al., 1996; Hizal et al., 2016; Yoda et al., 2014). Few studies have investigated the impacts of microscale surface roughness on biofilm growth, even though microscale surface roughness is ubiquitous in natural and artificial environments, such as the surfaces of sand beds in rivers (Hrvciw et al., 2016; Miller et al., 2014), drinking water pipelines (Niquette et al., 2000), and MBBRs (Mahto & Das, 2022; Morgan-Sagastume, 2018). The goal of this study is to fill the above research gaps and develop a mechanistic understanding of the impacts of hydrodynamic conditions and microscale surface roughness on the thickness of and the critical conditions to develop early-stage Pseudomonas putida biofilms.

We choose P. putida as our model organism because P. putida biofilms have been found on the surfaces of aquatic sediment (Brettar et al., 1994), terrestrial soils (Molina et al., 2000), and drinking water systems (Maes et al., 2020). P. putida has also been used as an environmental friendly bacterium for bioremediation and biodegradation (Pedersen et al., 1997; Samanta et al., 2002) due to its capability to degrade a wide variety of contaminants including lignin (Ravi et al., 2017; Xu et al., 2018), heavy metals (De et al., 2014; Imron et al., 2019), phenols (El-Naas et al., 2009) and naphthalene (Hwang et al., 2010). In addition, recent studies show that P. putida can kill bacterial competitors and protect tomato plants, suggesting that it can be used for pest control and sustainable agriculture (Purtschert-Montenegro et al., 2022). Due to the above applications, we choose P. putida as our model organism to reveal fundamental understanding of the physical factors that control the growth of early-stage biofilms.

SIOTECHNOLOGY -WILEY 3

In this study, we combined biofilm development experiments in custom-designed microfluidic channels, COMSOL simulations, and fluid mechanics theories to evaluate the impacts of hydrodynamic conditions and surface roughness on the critical shear stress, above which biofilms cease to form, and the thickness of early-stage *P. putida* biofilms. First, we investigate the influences of flow velocity and shear stress on biofilm thickness. Second, we quantify the impacts of the size and shape of microscale surface roughness on biofilm thickness. Third, we characterize the impacts of microscale surface roughness on the critical shear stress.

2 | MATERIALS AND METHODS

2.1 | Bacterial strain and growth medium

We cultivated *P. putida* KT-2442 (a gift from Mohamed Donia's lab, Princeton University) cells from frozen stocks in LB solution overnight (around 18 h) in an incubator with 200 rpm shaking rate at 30°C. Then, we transferred the cells in the growth phase to a modified M9 solution which has fully characterized chemical composition (Yang et al., 2021). The detailed information of bacterial culture was provided in Supporting Information: Text S1.

2.2 | Microfluidic experiments to measurement biofilm development

Microfluidic experiments were conducted to characterize biofilm development on smooth and rough surfaces under varied shear stress. Schematic diagram of the microfluidic platform is shown in Figure 1a. The system consists of a microfluidic chip, a confocal laser scanning microscope (CLSM) (Nikon C2 plus) and a syringe pump (PHD Ultra, Harvard Apparatus). Soft lithography was used to fabricate the microfluidic chip. The detailed information of soft

lithograph was provided in Supporting Information: Text S2. The microfluidic channel height $h=60~\mu m$, the channel width $D=400~\mu m$, and the channel length L=5~mm. During the experiments, the chips were placed on a stage top incubator (UNO-T-H, Okolab) with controlled temperature (30°C), which is the optimum temperature for P.~putida to grow (Fonseca et al., 2011). A syringe pump (PHD Ultra, Harvard Apparatus) was used to precisely control the injection rate of the nutrient solution. Confocal microscopy was used to image the biofilms in microfluidic channels with $0.31~\mu m/pixel$ resolution. The detailed information of confocal laser scanning microscopy was provided in Supporting Information: Text S3.

Biofilm development experiments were conducted following the steps below. First, we injected 500 µLP. putida solution (overnight cultures diluted with glucose-free M9 solution) with $OD_{600} = 0.48 \pm 0.05$ and a cell density of $(1.7 \pm 0.1) \times 10^8$ cells/mL into the microfluidic channel manually with flow rate on the order of mL/min. This bacterial concentration is similar to the values reported in DWDS, which are on the order of 10⁷ cells/mL (Rożei et al., 2015). Then, the P. putida solution in the channel was left undisturbed for 30 min to allow the cells attached to the surfaces. The glucose-free M9 solution was used to ensure that the number of cells attached to the microfluidic surfaces is the same for all surfaces at the beginning of the biofilm development experiments. Afterward, we injected abiotic M9 solution containing 1 wt. % (weight/weight percent) glucose at seven flow rates, from 1 µL/min to 125 $\mu L/min$ (τ_{avg} from 0.006 \pm 0.001 Pa to 0.84 \pm 0.16 Pa), to the channel using a syringe pump for 24 h. The range of shear stress values here are consistent with the values reported in drinking water distribution networks, which are in the range of 0.002-0.10 Pa (Gibson et al., 2020). As biofilms develop on the channel boundaries, we recorded time-lapse images of biofilms using a confocal microscope at 30-min intervals. To further demonstrate the existence of EPS within biofilms, we stained the EPS at the end of several selected experiments (Supporting Information: Figure S1). For the majority of the experiments, the

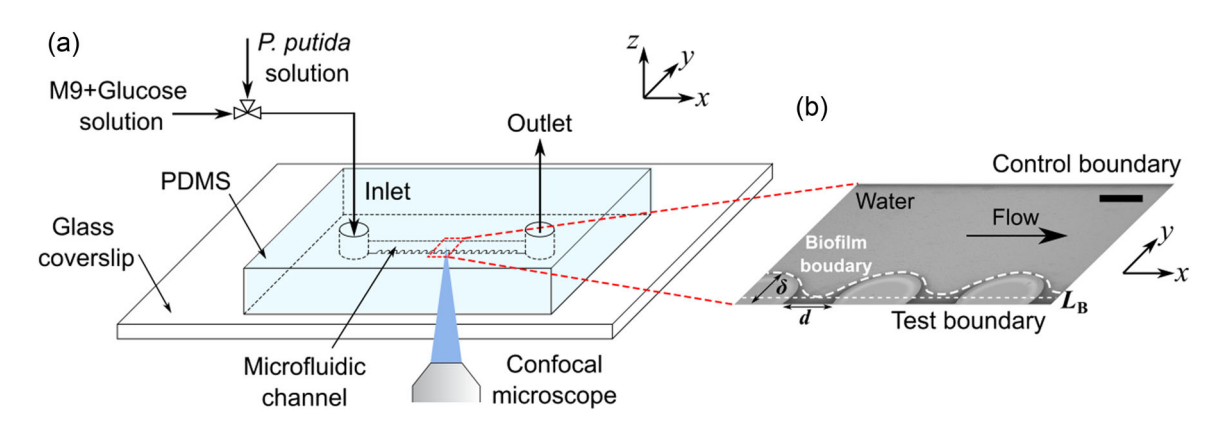


FIGURE 1 (a) Schematic diagram of the experimental setup. (b) Cross-sectional image of the microfluidic channel. Biofilms (gray color) accumulated at the control and test boundaries of the channel. $\delta = 100 \, \mu m$ denotes the height of the roughness elements at the test boundary. The distance between the neighboring roughness elements for all cases is the same, that is, $d = 100 \, \mu m$. L_B denotes the average biofilm thickness in the horizontal plane (x-y plane) grow perpendicular to the sidewall of the channel. (x is the flow direction, y is the lateral direction, and z is the vertical direction and the direction of gravity). The scale bar is $100 \, \mu m$.



biofilms were imaged using white-field function of the confocal microscope, and no dyes were used.

2.3 | The design of the microfluidic channels

To evaluate the impacts of surface roughness on biofilm development, we designed microfluidic channels with flat/smooth boundaries and rough boundaries with round and angular profile roughness structures (Figure 1). The roughness elements were placed at the test boundary of the microfluidics channel and the control boundary was flat for comparison (Figure 1b). Specifically, we fabricated circular and rectangular roughness structures with height $\delta = 100 \,\mu m$ (Figure 1b) to simulate the round and angular micron-size sediments in natural rivers (grain sizes on the order of 100 µm) (Garwood et al., 2013; Kadivar et al., 2021), microscale round and angular roughness geometries (surface roughness around 150 µm) in water pipes (Hall, 2017; Herwig et al., 2008; Niquette et al., 2000) and microscale surface roughness structures (average surface roughness >70 µm) used in bioreactor carriers (Bolton et al., 2006; Dong et al., 2015). The central distance between neighboring roughness elements (round and angular) was a constant, that is, $d = 100 \,\mu\text{m}$.

2.4 | Image analysis

Confocal microscope images were saved on a workstation (HP-Z4-G4). To calculate the biofilm thickness $L_{\rm B}$ in the horizontal plane (x-y plane in Figure 1b) perpendicular to the sidewalls of the channel, we first converted the confocal images to grayscale images and determined the threshold of color difference between biofilm boundary and water in Image-J. Then, we applied this threshold to determine the biofilm boundaries by subtracting the biofilm images with the background image (the first image of the time series experiments) using MATLAB. Afterward, the pixel intensities of the biofilm region were summed up and the average biofilm thickness $L_{\rm B}$ was determined by dividing the total pixel intensities by the length of the field of view.

2.5 | Numerical simulation

We simulated the flow in the microfluidic channel in two dimensions using computational fluid dynamics (CFD) finite-element simulation software, COMSOL Multiphysics 5.5. The geometry of the microfluidic channel was set the same as our experimental setup. The Navier-Stokes equation was numerically solved for flow velocity profiles inside the channel using no-slip boundary conditions on all solid boundaries. The stationary simulation was conducted in the fluid phase. Fully developed flow was assumed at the inflow and zero pressure was used at the outflow. Shear rate and shear stress distributions were calculated based on the velocity profiles in COMSOL. Note that Sanfilippo et al. (2019) pointed out that bacteria sense shear rate instead of shear stress. In our study, we used shear

stress because the viscosity of the fluid (which is water) is a constant during the experiments. We defined the spatially-averaged shear stress τ_{avg} as the mathematical mean value of the shear stress over the whole channel domain, which was calculated based on the shear stress distribution. More physical parameters used in COMSOL simulation are listed in Supporting Information: Table S1.

2.6 | Statistical analysis

The results of biofilm thickness are shown as mean ± standard error. The mean value of the biofilm thickness was calculated from the inlet, outlet, and middle part of the microfluidic channel. At least one biological replicate was conducted for all the roughness types. The error bars indicate standard error of four measurements. Regression analysis was conducted using MATLAB to predict the critical shear stress under different roughness types and identify the confidence level. More details are listed in Supporting Information: Table S2.

3 | RESULTS AND DISCUSSION

3.1 | Impacts of hydrodynamic conditions on biofilm thickness

To reveal the impacts of hydrodynamic conditions on the development of early-stage P. putida biofilms, we grew P. putida cells on the surfaces of custom-built microfluidic channels and measured the thickness of biofilms on the test boundary as a function of bacterial growth time (Figure 2a). Specifically, we first seeded the microfluidic channel with P. putida cells by injecting carbon-free bacterial solution with OD_{600} = 0.48 ± 0.05 into the microfluidic chamber with flat sidewalls for 30 min. Afterward, we switched to inject the cell-free nutrient solution (M9 medium with 1 wt. % glucose) continuously to allow the cells to grow and biofilms to develop. During the biofilm growth period, we scanned the microfluidic channel using a confocal laser scanning microscope (CLSM) and measured the average thickness of the biofilms developed on the test boundary over time at seven flow rates (shear stress τ_{avg} from $0.006 \pm 0.001 \, Pa$ to $0.84 \pm 0.16 \, Pa$) (Supporting Information: Figure \$3). Biofilms started to form on the test boundaries after 6-8 h of nutrient injection. Here, we focus on the early-stage biofilms with 14-h growth period, because compared with mature biofilms, early-stage biofilms are more sensitive to antimicrobials and changes in the environment and thus are easier to disrupt and control (Fu et al., 2021; Gu et al., 2019). For mature biofilm with a longer growth period, experiments with longer growth time are needed, which are beyond the scope of this work.

First, we demonstrated the impacts of shear stress on biofilm thickness developed on the flat test boundary. At the low shear stress range (0.005–0.03 Pa), we observed rapid increase in biofilm thickness over the 14-h growth period of early-stage biofilms (Figure 2a). The biofilm thickness increased exponentially from 8 to 14 h, indicating that biofilm development is contributed by exponential increase of cell

10970290, 0, Downloaded from https://onlinelibrary.wiley.com/doi/10.1002/bit.28409, Wiley Online Library on [27/04/2023]. See the Terms and Conditions (https://onlinelibrary.wiley.com/terms-and-conditions) on Wiley Online Library for rules of use; OA articles are governed by the applicable Creative Commons Licensee (Commons Licensee).

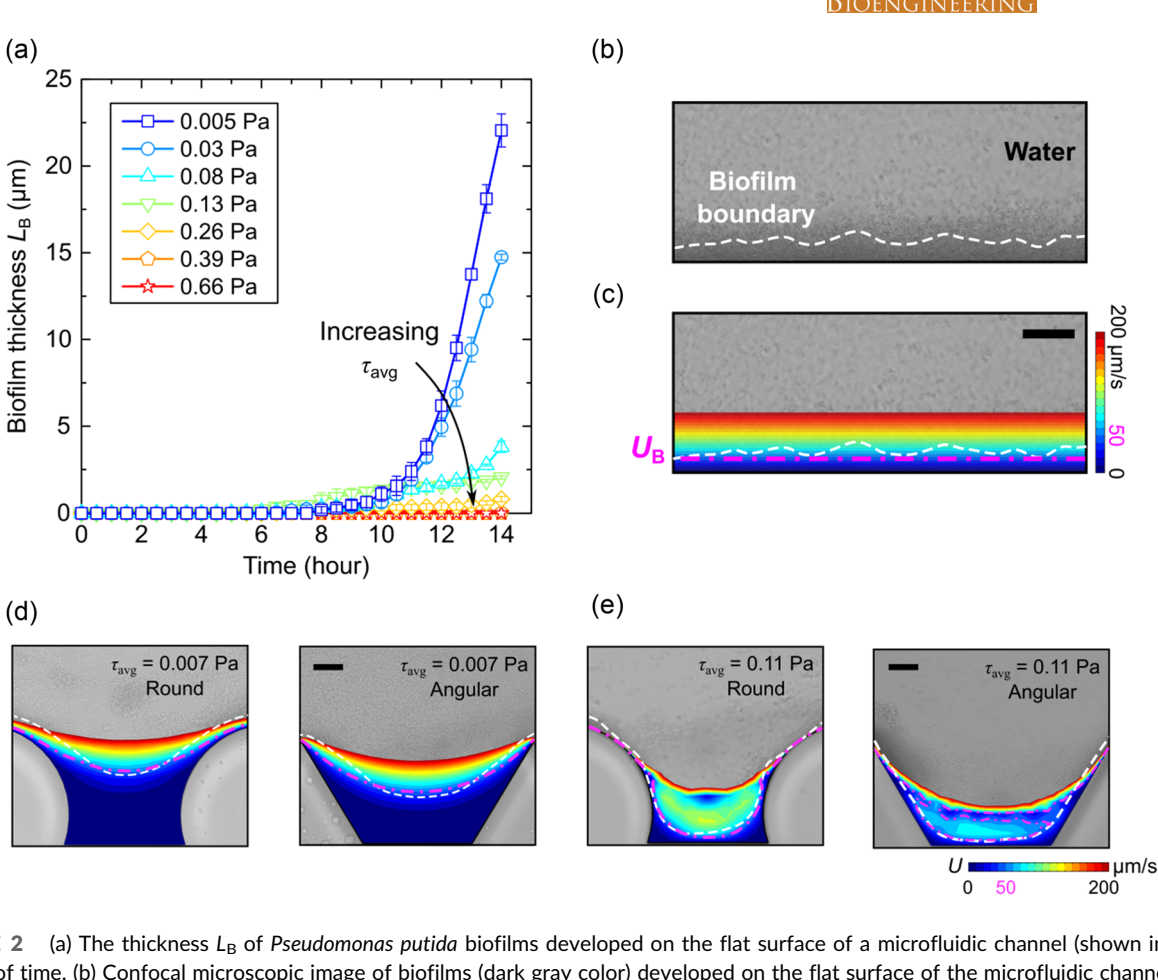


FIGURE 2 (a) The thickness L_B of *Pseudomonas putida* biofilms developed on the flat surface of a microfluidic channel (shown in b) as a function of time. (b) Confocal microscopic image of biofilms (dark gray color) developed on the flat surface of the microfluidic channel at shear stress $\tau_{avg} = 0.005$ Pa. The white dashed curve denotes the boundary of the biofilm accumulation region identified based on contrast of pixel intensity using Image-J. (c) Flow velocity distribution in color superimposed on gray-scale confocal image shown in (b). The pink dot-dashed line denotes the line with velocity equal to $50 \, \mu \text{m/s}$, which is the local velocity U_B for biofilm to develop. Images of flow velocity in color superimposed on gray-scale confocal images of early-stage biofilms on rough surfaces with round and angular roughness elements at shear stress $\tau_{avg} = 0.007$ Pa (d) and $\tau_{avg} = 0.11$ Pa (e). The scale bar is $25 \, \mu \text{m}$.

density during the growth phase (Drescher et al., 2013) (Supporting Information: Figure \$4). At middle shear stress range (0.08-0.13 Pa), the biofilm thickness did not increase exponentially over time and was smaller than the thickness of those grown under the low shear stress range. At the high shear stress range (0.26-0.66 Pa), no biofilms were observed at the test boundary, indicating that early-stage P. putida biofilms ceased to develop when the shear stress is above 0.26 Pa. In addition, we calculated the cell density on the test boundary and found that the cell density also decreased with increasing shear stress (Supporting Information: Text S4, Figure S5). The dependency of cell density on shear stress is consistent with the dependency of biofilm thickness on shear stress, further confirming that P. putida biofilms ceased to develop when the shear stress is above a critical value. The inhibition of early-stage biofilm development by high flow is likely because bacterial cells can be swept away by flow and detach from surfaces when the flow velocity or shear stress is higher than a critical value (Paul et al., 2012).

Second, by comparing the CLSM images of biofilms with the flow field simulation using COMSOL (Figure 2b,c), we found that

early-stage P. putida biofilms consistently accumulated at regions with flow velocities less than 50 μm/s (the pink lines in Figure 2c). The boundaries of biofilms (indicated by the white dashed lines in Figure 2b,c), coincide with the lines with local flow velocity equal to 50 µm/s (pink dashed lines in Figure 2b,c), indicating that the local velocity for the early-stage P. putida biofilms to develop is approximately $U_{\rm B}$ = 50 μ m/s. In addition, we conducted the same analysis for channels with varying roughness types at different shear stresses (Figure 2d,e) and found that the biofilm boundaries coincide with the contour of U_B regardless of shear stress and surface roughness (Supporting Information: Figure S6). Furthermore, the local velocity for biofilms to develop, 50 μm/s, is similar to P. putida's swimming speed, around 44 µm/s (Ping et al., 2013). Accordingly, we anticipate that biofilms cease to grow when the local fluid velocity exceeds the bacterial swimming speed, because bacterial cells can easily be swept away by flow and fail to attach to exiting biofilms when the flow velocity is greater than their swimming speed. Note that in the simulation, we assumed that biofilms do not affect the flow in the channel, which should only be valid for early-stage

highly-porous biofilms. Therefore, the observation that the boundary of biofilms occurred at locations with velocity similar to bacterial swimming speed may not be valid for more mature or denser biofilms (e.g., *P. putida* biofilms with growth time much larger than 14 h).

3.2 | Impacts of microscale surface roughness on biofilm thickness

Next, we evaluated the impacts of microscale surface roughness on early-stage biofilm growth by comparing the development of biofilms on surfaces of varying roughness in microfluidic channels (Supporting Information: Figure S3). Specifically, we measured the time evolution of the average thickness of biofilms developed on flat surface and rough surfaces with round and angular roughness elements (Figure 3a). The average biofilm thickness here was defined as the effective thickness assuming a flat surface, which is equal to the area of biofilm in 2D divided by the straight-line length of the boundary. As shown in Figure 3a, at the same shear stress, the average thickness of biofilms developed on rough surfaces at 14 h (L_{B-14 h}) is consistently larger. The increase on average biofilm thickness with rough surfaces is likely caused by the increase in the area of low velocity and shear regions induced by the surface roughness (Figure 3b,c). Above a flat surface, the streamline is parallel to the surfaces (Figure 2c), such that the region with velocity smaller than $U_{\rm B}$, the local velocity for early-stage P. putida biofilms to develop, is a thin rectangular region near the flat surface. In comparison, in channels with rough surface, regions with velocities smaller than $U_{\rm B}$ include the sheltered regions between the roughness elements, which provide shelter for bacterial cells to form biofilms (Figure 3b). In short, we demonstrated that microscale surface roughness promotes early-stage biofilm development, that is, increases average biofilm thickness by increasing the area of low-flow regions which provide shelter for the bacteria to form biofilms. Furthermore, we evaluated the impacts of different shapes of surface roughness on biofilm development. For the same roughness height, the average thickness of biofilms developed on surface with angular roughness elements is consistently larger, by up to about two times ($\tau_{avg} = 0.33$ ± 0.06 Pa case) than that for surface with round roughness (Figure 3a), suggesting that surface with angular roughness can further promote biofilm development compared with round shape. Detailed discussion of the impacts of roughness shape on biofilm development can be found in Supporting Information: Text \$5.

3.3 | Impacts of surface roughness on the critical condition to develop *P. putida* biofilms

Third, we characterized the impacts of microscale surface roughness on the spatially-averaged critical shear stress τ_{crit} , above which early-stage biofilms cease to develop. To start with, we used fluid mechanics theories to calculate $\tau_{crit-theo}$ for biofilms to develop on a flat surface from U_B . For the biofilm development experiments in

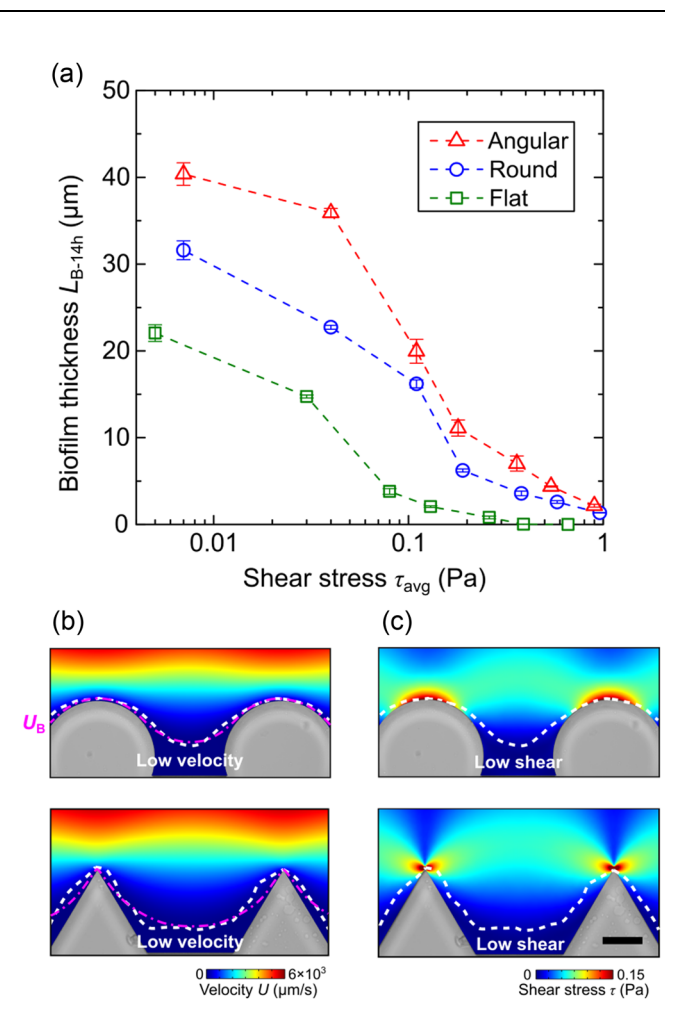


FIGURE 3 (a) The average thickness of early-stage *Pseudomonas putida* biofilms developed on flat and rough surfaces with round and angular elements at varying shear stress after 14 h growth period. The symbols and error bars represent the mean value and standard error of the biofilm thickness obtained from four replicate measurements respectively. Simulated velocity (b) and shear stress distribution (c) in color superimposed on gray-scale confocal images of biofilms in microfluidic channels with round and angular roughness elements (shear stress τ_{avg} = 0.007 Pa). The white dashed curve denotes the boundary of the biofilm. The pink dot-dashed line denotes the line with velocity equal to 50 μ m/s, which is the local velocity for biofilm to develop U_B . The scale bar is 50 μ m.

the microfluidic channel with channel width $D=400~\mu m$ at flow rate Q (Figure 4a), the Reynolds number $Re=\rho UD_h/\mu$ is at the range of 0.1–11.3, thus the flow is laminar (ρ is the density of water, U is the velocity at the inlet, $D_h=2Dh/(D+h)$ is the hydraulic diameter, $h=60~\mu m$ is the channel height, μ is the dynamic viscosity of water). Here, we assume that the early-stage P. putida biofilms are highly porous and as such do not affect the velocity distribution in the channel. In addition, we assume a fully developed flow, so the velocity profile follows the parabolic distribution of Hagen-Poiseuille flow (Bejan, 2013; Sutera & Skalak, 1993):

$$U = \frac{3Q[1-(2y/D)^2]}{2A},$$
 (1)

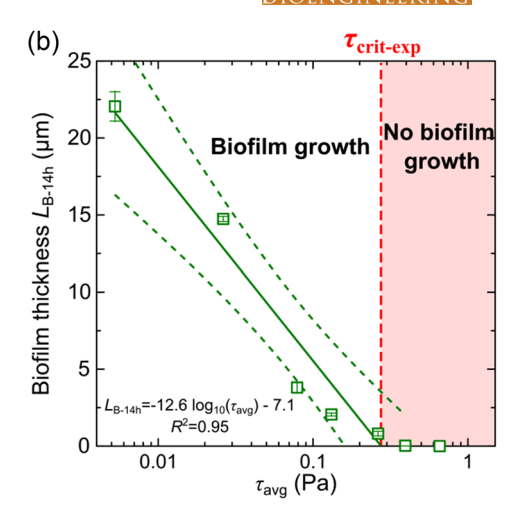


FIGURE 4 (a) Schematic diagram of the theoretical parabolic velocity distribution (black curve, Equation 1) in the microfluidic channel with flat surfaces. U_B denotes the local velocity for biofilms to develop and L_B denotes the biofilm thickness. The green color represents the region where bacterial biofilms accumulate. (b) The biofilm thickness L_{B-14h} measured from confocal images (after 14-h growth period) as a function of the shear stress τ_{avg} calculated from computational fluid dynamics (CFD) simulation. The red dashed line indicates the critical shear stress $\tau_{crit-exp} = 0.3$ Pa determined by experiment data, above which biofilms cease to develop on the flat surface. The solid green line indicates the linear fit L_{B-14h} (μ m) = -12.6 log₁₀ (τ_{avg} (Pa)) -7.1. The green dashed line represents the 90% confidence interval.

where $A = 0.024 \,\mathrm{mm}^2$ is the cross-section area of the channel. Assuming that early-stage biofilms only develop in regions with velocity less than U_{B} (Figure 2c), the thickness of biofilms, L_{B} , on the flat surface can be estimated by substituting U_{B} into Equation (1):

$$L_{\rm B} = \frac{D}{2} \cdot \frac{D}{2} \sqrt{1 - \frac{2U_{\rm B}A}{3Q}} \,. \tag{2}$$

We assumed that no biofilm will develop on the flat surface when the thickness of this low-velocity zone $L_{\rm B}$ is less than 1/10 of the bacterial width, which is 0.1 μ m for *P. putida* (Davis et al., 2011). Combining $L_{\rm B}$ = 0.1 μ m and Equations (1) and (2), the critical shear stress $\tau_{\rm crit-theo}$ to develop biofilms can be estimated as:

$$\tau_{\text{crit-theo}} = \mu \frac{dU}{dy} \bigg|_{y=D/2} = \frac{4\mu U_{\text{B}}}{D[1-(1-2L_{\text{B}}/D)^2]}.$$
 (3)

The above equation is the derived theoretical critical shear stress $\tau_{\text{crit-theo}}$ for *P. putida* biofilms to develop on a flat surface. Note that the nutrient solution we flow into the microfluidic cells is cell-free, so the development of biofilms is due to the growth of cells, which is different from Drescher et al. (2013) that assumes that the growth of biofilm streamers was due to the attachment of cells to existing streamers. From Equation (3), we predicted that the theoretical critical shear stress for *P. putida* biofilms to develop on a flat surface is $\tau_{\text{crit-theo}}$ = 0.4 Pa. To test the validity of our critical shear stress theory (Equation 3), we compared the predicted critical shear stress $\tau_{\text{crit-theo}}$ = 0.4 Pa with the critical stress estimated from our measurements. Specifically, we plotted the measured average thickness of biofilms developed on the flat surface at 14-h growthtime, $L_{\text{B-14h}}$, versus the shear stress τ_{avg} calculated from the CFD simulation results (Figure 4b). Our results showed that $L_{\text{B-14h}}$

decreased with increasing log_{10} (τ_{avg}) and above a certain critical shear stress, no biofilms were observed on the surface. The cell density we measured also confirmed that the biofilm growth will be inhibited above a certain critical shear stress (Supporting Information: Figure \$5). To estimate this critical shear stress, we fitted a linear line (green line in Figure 4b) to the L_{B-14h} versus log_{10} (τ_{avg}) data, from which we identified that the x-intercept is 0.3 Pa. This x-intercept is the critical shear stress $\tau_{\text{crit-exp}}$ for biofilms to develop on a flat surface. The agreement between $\tau_{crit-exp}$ = 0.3 Pa based on measurements and the $\tau_{crit-theo}$ = 0.4 Pa based on theoretical calculation (Equation 3) confirms our hypothesis that the critical conditions to develop biofilms is controlled by local flow velocity. Our measured $\tau_{crit-flat}$ = 0.3 Pa is also consistent with some previous studies using other microorganisms (e.g., Belohlav et al., 2020; Roosjen et al., 2005). For example, the critical shear stress for microalgae Chlorella vulgaris biofilms to develop on the flat surface of photobioreactor panel is 0.2 Pa (Belohlav et al., 2020) and the critical shear stress to prevent adhesion for the yeast strains on smooth glass is 0.36 Pa (Roosjen et al., 2005). Note that here we assume that early-stage biofilms are highly porous and do not affect the flow field. This assumption may not apply to more mature biofilms at later stages (e.g., with growth time much longer than 14 h), which are denser and can alter the flow field in the channel (Greener et al., 2016; Nguyen et al., 2005). For these denser and mature biofilms, the impacts of biofilms on the flow need to be considered (e.g., Brito & Melo, 1999; De Beer et al., 1996; Greener et al., 2016; Nguyen et al., 2005).

Furthermore, we demonstrated the impacts of surface roughness on $\tau_{crit}.$ We plotted the average biofilm thickness as a function of the average shear stress (Figure 5) and identified τ_{crit} for each rough surface. Compared with the flat surfaces for which the measured $\tau_{crit\text{-flat}}$ = 0.3 Pa, the τ_{crit} for biofilms to develop on surfaces with

round roughness is 0.8 Pa and on surfaces with angular roughness is 0.9 Pa. Therefore, the critical shear stress τ_{crit} for P. putida biofilms to develop on surfaces with microscale roughness is about three times as large as that for flat surface. Our results highlight the important

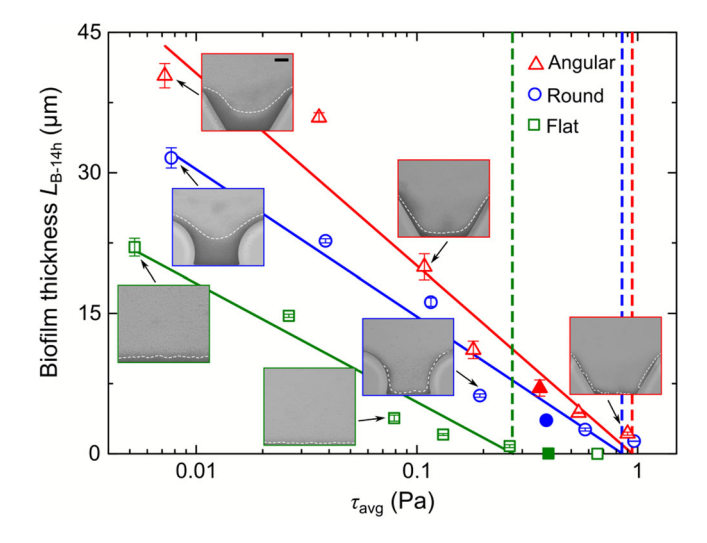


FIGURE 5 Measured biofilm thickness after 14-h growth period L_{B-14h} as a function of average shear stress τ_{avg} for flat surface (green) and rough surfaces with round elements (blue) and angular elements (red). The dashed vertical lines indicate the critical shear stress for the flat surface $\tau_{crit\text{-flat}}$ (green), surfaces with round roughness $\tau_{crit\text{-round}}$ (blue), and angular roughness $\tau_{crit\text{-angular}}$ (red). The three symbols filled with color represent the data (τ_{avg} = 0.38 ± 0.02 Pa) used for Figure 6. The insets show confocal images for representative cases indicated by the black arrows. The scale bar on the top left image is 25 µm and all insets have the same scale bar.

control of microscale surface roughness on early-stage P.~putida biofilm development and the critical shear stress required to inhibit early-stage P.~putida biofilm growth. We caution that τ_{crit} may be different for different bacterial species, different growth time, and on different substrate surfaces. For example, proteobacterium Geobacter sulfurreducens can form 41 μ m-thick biofilms (after 7 days) when the wall shear stress is 1 Pa (Jones & Buie, 2019). The critical shear stress for Staphylococcus epidermidis biofilms to develop on silicone rubber surface is 2.7 Pa and on PEO-coated silicone rubber is 0.2 Pa (Nejadnik et al., 2008). The critical shear stress for mature Pseudomonas~aeruginosa~biofilms in flat microfluidic channels before sloughing (after 50 h) is 1.4 Pa (Greener et al., 2022), the same order of magnitude as the value for the early-stage P.~putida~biofilms (0.3 Pa) in our study.

Given the critical shear stress τ_{crit} that prevent biofilm development, the critical hydrodynamic force exerted on a single cell to remove bacterial adhesion can be estimated as $F = \tau_{crit} A_c$, with $A_c = 3.14 \, \mu m^2$ the area of one single *P. putida* cell exposed to the flow (Davis et al., 2011). Therefore, the critical adhesion force for *P. putida* cell to attach to a flat/smooth PDMS surface is $F = 0.3 \, \text{Pa} \times 3.14 \, \mu m^2 = 0.9 \, \text{pN}$, and the critical adhesion force for a rough surface is $F = 0.9 \, \text{Pa} \times 3.14 \, \mu m^2 = 2.8 \, \text{pN}$. Consistently, Nejadnik et al. (2008) used a similar method and identified the critical forces to remove *S. epidermidis* from PEO-coated and pristine silicone rubber is 0.1 and 2.1 pN, respectively, which are the same orders of magnitude as our results. Other studies used atomic force microscopy (AFM) to directly measure adhesion forces between the cells and surfaces (Hizal et al., 2016; Xu et al., 2005), which is in the nN range. Such difference is because AFM measures the forces perpendicular to the surface

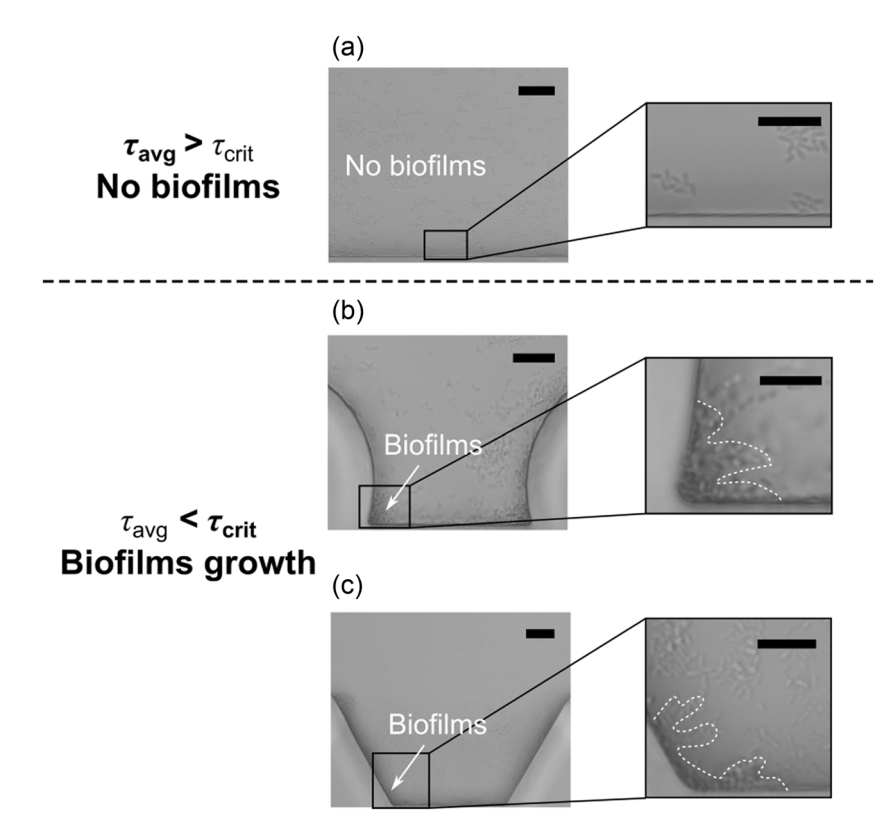


FIGURE 6 Confocal images of biofilms on flat and rough surfaces under a similar average shear stress (τ_{avg} = 0.38 ± 0.02 Pa). (a) On the flat surface, no biofilm developed on the surfaces because the average shear stress τ_{avg} is larger than the critical shear stress $\tau_{crit\text{-flat}}$ = 0.3 Pa. On surfaces with round roughness (b) and angular roughness (c) at a similar shear stress, biofilms were observed on surfaces. This is because for rough surfaces the shear stress τ_{avg} is smaller than the critical shear stress $\tau_{crit\text{-rough}}$ = 0.85 ± 0.05 Pa. The white dashed lines denote the boundaries of biofilms based on contrast of pixel intensity using Image-J. The scale bar on the left images is 25 µm. The scale bar of zoom-in images is 10 µm.

under static conditions, while the estimated critical hydrodynamic force ($F = \tau_{crit} A_c$) is tangential to the surface under flow conditions (Nejadnik et al., 2008).

At a similar shear stress, for example, $\tau_{avg} = 0.38 \pm 0.02 \, \text{Pa}$, we anticipated that no early-stage P. putida biofilms would develop on the flat surface, because the τ_{avg} is larger than $\tau_{crit-flat}$ = 0.3 Pa (Figure 6). In contrast, we predicted that biofilms would develop on the rough surfaces with both angular and round roughness elements, because the τ_{avg} = 0.38 ± 0.02 Pa is smaller than $\tau_{crit-rough}$ = 0.85 ± 0.05 Pa for rough surface with round and angular roughness shapes. Our predictions are confirmed by our microfluidic observations that biofilms indeed developed on rough surfaces under a similar average shear stress ($\tau_{avg} = 0.38 \pm 0.02 \,\text{Pa}$), as shown in Figure 6. The above observations demonstrate that surface roughness does increase τ_{crit} and as such it is more difficult to prevent early-stage biofilm growth on surfaces with microscale roughness than smooth surfaces. Compared with smooth surfaces, a larger shear stress is required to prevent biofilm growth on rough surfaces, such as the rough surfaces of angular sediment deposits in fluvial system (Nejadnik et al., 2008), drinking water pipes (Fish et al., 2017), and MBBRs used in wastewater treatment plants (Morgan-Sagastume, 2018).

4 | CONCLUSIONS

Our study highlights the important roles of hydrodynamic conditions and microscale surface roughness in controlling the early-stage development of P. putida biofilms and provides systematic and quantitative characterization of these effects. First, we show that early-stage P. putida biofilm growth is suppressed under high-flow conditions. By combining experimental and simulation results, we demonstrate that the local velocity for early-stage P. putida biofilms, after 14-h growth time, to develop is 50 µm/s, which is similar to P. putida's swimming speed. Furthermore, we reveal the impacts of microscale surface roughness on the early-stage biofilm growth. We show that roughness elements create sheltered low-flow regions that promote biofilm development. Compared with the surface with round roughness elements, angular roughness elements provide larger area of low-flow region, which further facilitate biofilm accumulation. Furthermore, we propose a theoretical model to predict the critical shear stress, above which early-stage biofilms cease to develop on flat surfaces, which is $\tau_{crit-flat} = 0.3 \, \text{Pa}$ for P. putida. The theory was validated with experimental measurements. Finally, we demonstrate that the critical shear stress for early-stage P. putida biofilms to develop on rough surfaces with angular and round roughness is 0.9 and 0.8 Pa, respectively, which are about three times as large as that for flat surface (0.3 Pa). We expect that the experimental methods and predictive equations developed in this study using a single-species biofilm can apply to other multispecies biofilms in the future.

AUTHOR CONTRIBUTIONS

Guanju Wei and Judy Q. Yang conceived and designed the project. Guanju Wei and Judy Q. Yang designed the experiments. Guanju Wei conducted the experiments. Guanju Wei and Judy Q. Yang analyzed the data and wrote the paper.

ACKNOWLEDGMENTS

This study was supported by Minnesota's Discovery, Research, and Innovation Economy (MnDRIVE) at the University of Minnesota and National Science Foundation EAR 2236497. Portions of this work were conducted in the Minnesota Nano Center, which is supported by the National Science Foundation through the National Nanotechnology Coordinated Infrastructure (NNCI) under Award Number ECCS-2025124. We thank Dr. J Sanfilippo for the strains.

CONFLICT OF INTEREST STATEMENT

The authors declare no conclict of interest.

DATA AVAILABILITY STATEMENT

Data are available in the Data Repository for the University of Minnesota repository (https://doi.org/10.13020/afnk-kp31).

ORCID

Guanju Wei http://orcid.org/0000-0001-5511-9242

Judy Q. Yang http://orcid.org/0000-0001-6272-1266

REFERENCES

- Abu Bakar, M., McKimm, J., Haque, S. Z., Majumder, A. A., & Haque, M. (2018). Chronic tonsillitis and biofilms: A brief overview of treatment modalities. *Journal of Inflammation Research*, 11, 329–337. https://doi.org/10.2147/JIR.S162486
- Armbruster, C. R., & Parsek, M. R. (2018). New insight into the early stages of biofilm formation. *Proceedings of the National Academy of Sciences United States of America*, 115(17), 4317–4319. https://doi.org/10.1073/pnas.1804084115
- Bassin, J. P., Kleerebezem, R., Rosado, A. S., van Loosdrecht, M. C., & Dezotti, M. (2012). Effect of different operational conditions on biofilm development, nitrification, and nitrifying microbial population in moving-bed biofilm reactors. *Environmental Science & Technology*, 46(3), 1546–1555. https://doi.org/10.1021/es203356z
- De Beer, D., Stoodley, P., & Lewandowski, Z. (1996). Liquid flow and mass transport in heterogeneous biofilms. *Water Research*, 30(11), 2761–2765. https://doi.org/10.1016/S0043-1354(96)00141-8
- Bejan, A. (2013). Convection heat transfer. John Wiley & Sons.
- Belohlav, V., Zakova, T., Jirout, T., & Kratky, L. (2020). Effect of hydrodynamics on the formation and removal of microalgal biofilm in photobioreactors. *Biosystems Engineering*, 200, 315–327. https://doi.org/10.1016/j.biosystemseng.2020.10.014
- Bester, E., Wolfaardt, G., Aznaveh, N., & Greener, J. (2013). Biofilms' role in planktonic cell proliferation. *International Journal of Molecular Sciences*, 14(11), 21965–21982. https://doi.org/10.3390/ijms1411 21965
- Bollen, C. M. L., Papaioanno, W., Van Eldere, J., Schepers, E., Quirynen, M., & Van Steenberghe, D. (1996). The influence of abutment surface roughness on plaque accumulation and peri-implant mucositis. Clinical Oral Implants Research, 7(3), 201–211. https://doi.org/10. 1034/j.1600-0501.1996.070302.x
- Bolton, J., Tummala, A., Kapadia, C., Dandamudi, M., & Belovich, J. M. (2006). Procedure to quantify biofilm activity on carriers used in wastewater treatment systems. *Journal of Environmental Engineering*, 132(11), 1422–1430. https://doi.org/10.1061/(ASCE)0733-9372 (2006)132:11(1422)



- Brettar, I., Ramos-Gonzalez, M. I., Ramos, J. L., & Höfle, M. G. (1994). Fate of *Pseudomonas putida* after release into lake water mesocosms: Different survival mechanisms in response to environmental conditions. *Microbial Ecology*, 27(2), 99–122. https://doi.org/10.1007/BF00165812
- Brito, A. G., & Melo, L. F. (1999). Mass transfer coefficients within anaerobic biofilms: Effects of external liquid velocity. *Water Research*, 33(17), 3673–3678. https://doi.org/10.1016/S0043-1354(99)00078-0
- De Carvalho, C. C. C. R. (2018). Marine biofilms: A successful microbial strategy with economic implications. Frontiers in Marine Science, 5, 126. https://doi.org/10.3389/fmars.2018.00126
- Chinnaraj, S. B., Jayathilake, P. G., Dawson, J., Ammar, Y., Portoles, J., Jakubovics, N., & Chen, J. (2021). Modelling the combined effect of surface roughness and topography on bacterial attachment. *Journal of Materials Science & Technology*, 81, 151–161. https://doi.org/10.1016/j.jmst.2021.01.011
- Cho, K. H., Wolny, J., Kase, J. A., Unno, T., & Pachepsky, Y. (2022). Interactions of E. coli with algae and aquatic vegetation in natural waters. Water Research, 209, 117952. https://doi.org/10.1016/j. watres.2021.117952
- Cowle, M. W., Webster, G., Babatunde, A. O., Bockelmann-Evans, B. N., & Weightman, A. J. (2020). Impact of flow hydrodynamics and pipe material properties on biofilm development within drinking water systems. *Environmental Technology*, 41(28), 3732–3744. https://doi.org/10.1080/09593330.2019.1619844
- Coyte, K. Z., Tabuteau, H., Gaffney, E. A., Foster, K. R., & Durham, W. M. (2017). Microbial competition in porous environments can select against rapid biofilm growth. *Proceedings of the National Academy of Sciences United States of America*, 114(2), E161–E170. https://doi. org/10.1073/pnas.1525228113
- Davey, M. E., & O'Toole, G. A. (2000). Microbial biofilms: From ecology to molecular genetics. Microbiology and Molecular Biology Reviews, 64(4), 847–867. https://doi.org/10.1128/MMBR.64.4.847-867.2000
- Davis, M. L., Mounteer, L. C., Stevens, L. K., Miller, C. D., & Zhou, A. (2011). 2D motility tracking of *Pseudomonas putida* KT2440 in growth phases using video microscopy. *Journal of Bioscience and Bioengineering*, 111(5), 605-611. https://doi.org/10.1016/j.jbiosc. 2011.01.007
- De, J., Leonhäuser, J., & Vardanyan, L. (2014). Removal of mercury in fixed-bed continuous upflow reactors by mercury-resistant bacteria and effect of sodium chloride on their performance. *QScience Connect*, 2014(1), 1–9. https://doi.org/10.5339/connect.2014.17
- Dong, Y., Fan, S., Shen, Y., Yang, J., Yan, P., Chen, Y., Li, J., Guo, J., Duan, X., & Fang, F. (2015). A novel bio-carrier fabricated using 3D printing technique for wastewater treatment. *Scientific Reports*, 5(1), 1–10. https://doi.org/10.1038/srep12400
- Donlan, R. (2001). Biofilms and device-associated infections. Emerging Infectious Diseases, 7(2), 277–281. https://doi.org/10.3201/eid07 02.010226
- Drescher, K., Shen, Y., Bassler, B. L., & Stone, H. A. (2013). Biofilm streamers cause catastrophic disruption of flow with consequences for environmental and medical systems. *Proceedings of the National Academy of Sciences United States of America*, 110(11), 4345–4350. https://doi.org/10.1073/pnas.1300321110
- Dressaire, E., & Sauret, A. (2017). Clogging of microfluidic systems. *Soft Matter*, 13(1), 37-48. https://doi.org/10.1039/C6SM01879C
- Drummond, J. D., Davies-Colley, R. J., Stott, R., Sukias, J. P., Nagels, J. W., Sharp, A., & Packman, A. I. (2015). Microbial transport, retention, and inactivation in streams: A combined experimental and stochastic modeling approach. *Environmental Science & Technology*, 49(13), 7825-7833. https://doi.org/10.1021/acs.est.5b01414
- El-Naas, M. H., Al-Muhtaseb, S. A., & Makhlouf, S. (2009). Biodegradation of phenol by *Pseudomonas putida* immobilized in polyvinyl alcohol

- (PVA) gel. Journal of Hazardous Materials, 164(2), 720–725. https://doi.org/10.1016/j.jhazmat.2008.08.059
- Fish, K., Osborn, A. M., & Boxall, J. B. (2017). Biofilm structures (EPS and bacterial communities) in drinking water distribution systems are conditioned by hydraulics and influence discolouration. *Science of the Total Environment*, 593–594, 571–580. https://doi.org/10.1016/j.scitotenv.2017.03.176
- Fonseca, P., Moreno, R., & Rojo, F. (2011). Growth of *Pseudomonas putida* at low temperature: Global transcriptomic and proteomic analyses. *Environmental Microbiology Reports*, 3(3), 329–339. https://doi.org/10.1111/j.1758-2229.2010.00229.x
- Fu, J., Zhang, Y., Lin, S., Zhang, W., Shu, G., Lin, J., Li, H., Xu, F., Tang, H., Peng, G., Zhao, L., Chen, S., & Fu, H. (2021). Strategies for interfering with bacterial early stage biofilms. *Frontiers in Microbiology*, 12, 1339. https://doi.org/10.3389/fmicb.2021.675843
- Garwood, J. C., Hill, P. S., & Law, B. A. (2013). Biofilms and size sorting of fine sediment during erosion in intertidal sands. *Estuaries and Coasts*, 36(5), 1024–1036. https://doi.org/10.1007/s12237-013-9618-z
- Geisel, S., Secchi, E., & Vermant, J. (2022). The role of surface adhesion on the macroscopic wrinkling of biofilms. *eLife*, 11, e76027. https://doi. org/10.7554/eLife.76027
- Ghannoum, M., Parsek, M., Whiteley, M., & Mukherjee, P. K. (2020). *Microbial Biofilms*. John Wiley & Sons.
- Gibson, J., Karney, B., & Guo, Y. (2020). Effects of relaxed minimum pipe diameters on fire flow, cost, and water quality indicators in drinking water distribution networks. *Journal of Water Resources Planning and Management*, 146(8), 4020059. https://doi.org/10.1061/(ASCE)WR. 1943-5452.0001251
- Greener, J., Harvey, W. Y., Gagné-Thivierge, C., Fakhari, S., Taghavi, S. M., Barbeau, J., & Charette, S. J. (2022). Critical shear stresses of Pseudomonas aeruginosa biofilms from dental unit waterlines studied using microfluidics and additional magnesium ions. Physics of Fluids, 34(2), 021902. https://doi.org/10.1063/5.0076737
- Greener, J., Parvinzadeh Gashti, M., Eslami, A., Zarabadi, M. P., & Taghavi, S. M. (2016). A microfluidic method and custom model for continuous, non-intrusive biofilm viscosity measurements under different nutrient conditions. *Biomicrofluidics*, 10(6), 064107. https://doi.org/10.1063/1.4968522
- Gu, H., Lee, S. W., Carnicelli, J., Jiang, Z., & Ren, D. (2019). Antibiotic susceptibility of *Escherichia coli* cells during early-stage biofilm formation. *Journal of Bacteriology*, 201(18), e19–e34. https://doi. org/10.1128/JB.00034-19
- Hall, C. W., & Mah, T. F. (2017). Molecular mechanisms of biofilm-based antibiotic resistance and tolerance in pathogenic bacteria. FEMS Microbiology Reviews, 41(3), 276–301. https://doi.org/10.1093/ femsre/fux010
- Hall, S. (2017). Rules of thumb for chemical engineers. Butterworth-Heinemann.
- Herwig, H., Gloss, D., & Wenterodt, T. (2008). A new approach to understanding and modelling the influence of wall roughness on friction factors for pipe and channel flows. *Journal of Fluid Mechanics*, 613, 35–53. https://doi.org/10.1017/S0022112008003534
- Hizal, F., Choi, C. H., Busscher, H. J., & van der Mei, H. C. (2016). Staphylococcal adhesion, detachment and transmission on nanopillared Si surfaces. ACS Applied Materials & Interfaces, 8(44), 30430–30439. https://doi.org/10.1021/acsami.6b09437
- Hryciw, R. D., Zheng, J., & Shetler, K. (2016). Particle roundness and sphericity from images of assemblies by chart estimates and computer methods. *Journal of Geotechnical and Geoenvironmental Engineering*, 142(9), 4016038. https://doi.org/10.1061/(ASCE)GT. 1943-5606.0001485
- Hwang, G., Lee, C. H., Ahn, I. S., & Mhin, B. J. (2010). Analysis of the adhesion of *Pseudomonas putida* NCIB 9816-4 to a silica gel as a model soil using extended DLVO theory. *Journal of Hazardous*

10970290, 0, Downloaded from https://onlinelibrary.wiley.com/doi/10.1002/bit.28409, Wiley Online Library on [27/04/2023]. See the Terms and Conditions (https://onlinelibrary.wiley.com/terms-and-conditions) on Wiley Online Library for rules of use; OA articles are governed by the applicable Creative Commons Licensee

- Materials, 179(1-3), 983-988. https://doi.org/10.1016/j.jhazmat. 2010.03.101
- Imron, M. F., Kurniawan, S. B., & Soegianto, A. (2019). Characterization of mercury-reducing potential bacteria isolated from Keputih nonactive sanitary landfill leachate, Surabaya, Indonesia under different saline conditions. *Journal of Environmental Management*, 241, 113–122. https://doi.org/10.1016/j.jenyman.2019.04.017
- Janjaroen, D., Ling, F., Monroy, G., Derlon, N., Mogenroth, E., Boppart, S. A., Liu, W. T., & Nguyen, T. H. (2013). Roles of ionic strength and biofilm roughness on adhesion kinetics of *Escherichia* coli onto groundwater biofilm grown on PVC surfaces. Water Research, 47(7), 2531–2542. https://doi.org/10.1016/j.watres. 2013.02.032
- Jones, A. A. D., & Buie, C. R. (2019). Continuous shear stress alters metabolism, mass-transport, and growth in electroactive biofilms independent of surface substrate transport. *Scientific Reports*, 9(1), 2602. https://doi.org/10.1038/s41598-019-39267-2
- Kadivar, M., Tormey, D., & McGranaghan, G. (2021). A review on turbulent flow over rough surfaces: Fundamentals and theories. *International Journal of Thermofluids*, 10, 100077. https://doi.org/10. 1016/j.ijft.2021.100077
- Krsmanovic, M., Biswas, D., Ali, H., Kumar, A., Ghosh, R., & Dickerson, A. K. (2021). Hydrodynamics and surface properties influence biofilm proliferation. Advances in Colloid and Interface Science, 288, 102336. https://doi.org/10.1016/j.cis.2020.102336
- Lemos, M., Mergulhão, F., Melo, L., & Simões, M. (2015). The effect of shear stress on the formation and removal of *Bacillus cereus* biofilms. *Food and Bioproducts Processing*, *93*, 242–248. https://doi.org/10.1016/j.fbp.2014.09.005
- Liu, N., Skauge, T., Landa-Marbán, D., Hovland, B., Thorbjørnsen, B., Radu, F. A., Vik, B. F., Baumann, T., & Bødtker, G. (2019). Microfluidic study of effects of flow velocity and nutrient concentration on biofilm accumulation and adhesive strength in the flowing and noflowing microchannels. *Journal of Industrial Microbiology and Biotechnology*, 46(6), 855–868. https://doi.org/10.1007/s10295-019-02161-x
- Liu, Y., & Tay, J. H. (2002). The essential role of hydrodynamic shear force in the formation of biofilm and granular sludge. Water Research, 36(7), 1653–1665. https://doi.org/10.1016/S0043-1354(01)00379-7
- Maes, S., De Reu, K., Van Weyenberg, S., Lories, B., Heyndrickx, M., & Steenackers, H. (2020). Pseudomonas putida as a potential biocontrol agent against Salmonella Java biofilm formation in the drinking water system of broiler houses. BMC Microbiology, 20(1), 373. https://doi.org/10.1186/s12866-020-02046-5
- Mahto, K. U., & Das, S. (2022). Bacterial biofilm and extracellular polymeric substances in the moving bed biofilm reactor for wastewater treatment: A review. *Bioresource Technology*, 345, 126476. https://doi.org/10.1016/j.biortech.2021.126476
- Mielich Süss, B., & Lopez, D. (2015). Molecular mechanisms involved in *Bacillus subtilis* biofilm formation. *Environmental Microbiology*, 17(3), 555–565. https://doi.org/10.1111/1462-2920.12527
- Miller, K. L., Szabó, T., Jerolmack, D. J., & Domokos, G. (2014). Quantifying the significance of abrasion and selective transport for downstream fluvial grain size evolution. *Journal of Geophysical Research: Earth Surface*, 119(11), 2412–2429. https://doi.org/10.1002/2014JF003156
- Molina, L., Ramos, C., Duque, E., Ronchel, M. C., García, J. M., Wyke, L., & Ramos, J. L. (2000). Survival of *Pseudomonas putida* KT2440 in soil and in the rhizosphere of plants under greenhouse and environmental conditions. *Soil Biology and Biochemistry*, *32*(3), 315–321. https://doi.org/10.1016/S0038-0717(99)00156-X
- Morgan-Sagastume, F. (2018). Biofilm development, activity and the modification of carrier material surface properties in moving-bed biofilm reactors (MBBRs) for wastewater treatment. *Critical Reviews in Environmental Science and Technology*, 48(5), 439–470. https://doi.org/10.1080/10643389.2018.1465759

- Nejadnik, M. R., Van Der Mei, H. C., Busscher, H. J., & Norde, W. (2008). Determination of the shear force at the balance between bacterial attachment and detachment in weak-adherence systems, using a flow displacement chamber. *Applied and Environmental Microbiology*, 74(3), 916–919. https://doi.org/10.1128/AEM.01557-07
- Nguyen, V. T., Morgenroth, E., & Eberl, H. J. (2005). A mesoscale model for hydrodynamics in biofilms that takes microscopic flow effects into account. Water Science and Technology, 52(7), 167–172. https:// doi.org/10.2166/wst.2005.0197
- Niquette, P. (2000). Impacts of pipe materials on densities of fixed bacterial biomass in a drinking water distribution system. *Water Research*, 34(6), 1952–1956. https://doi.org/10.1016/S0043-1354 (99)00307-3
- Paquet-Mercier, F., Parvinzadeh Gashti, M., Bellavance, J., Taghavi, S. M., & Greener, J. (2016). Through thick and thin: A microfluidic approach for continuous measurements of biofilm viscosity and the effect of ionic strength. *Lab on a Chip*, 16(24), 4710–4717. https://doi.org/10. 1039/c6lc01101b
- Paramonova, E., Kalmykowa, O. J., Van der Mei, H. C., Busscher, H. J., & Sharma, P. K. (2009). Impact of hydrodynamics on oral biofilm strength. *Journal of Dental Research*, 88(10), 922–926. https://doi.org/10.1177/0022034509344569
- Parvinzadeh Gashti, M., Bellavance, J., Kroukamp, O., Wolfaardt, G., Taghavi, S. M., & Greener, J. (2015). Live-streaming: Time-lapse video evidence of novel streamer formation mechanism and varying viscosity. *Biomicrofluidics*, 9(4), 041101. https://doi.org/10.1063/1.4928296
- Paul, E., Ochoa, J. C., Pechaud, Y., Liu, Y., & Liné, A. (2012). Effect of shear stress and growth conditions on detachment and physical properties of biofilms. Water Research, 46(17), 5499–5508. https://doi.org/10. 1016/j.watres.2012.07.029
- Pedersen, A. R., Møller, S., Molin, S., & Arvin, E. (1997). Activity of toluene-degrading *Pseudomonas putida* in the early growth phase of a biofilm for waste gas treatment. *Biotechnology and Bioengineering*, 54(2), 131–141. https://doi.org/10.1002/(SICI)1097-0290(19970 420)54:2<131::AID-BIT5>3.0.CO;2-M
- Ping, L., Birkenbeil, J., & Monajembashi, S. (2013). Swimming behavior of the monotrichous bacterium *Pseudomonas fluorescens* SBW25. *FEMS Microbiology Ecology*, 86(1), 36–44. https://doi.org/10.1111/1574-6941.12076
- Purtschert-Montenegro, G., Cárcamo-Oyarce, G., Pinto-Carbó, M., Agnoli, K., Bailly, A., & Eberl, L. (2022). Pseudomonas putida mediates bacterial killing, biofilm invasion and biocontrol with a type IVB secretion system. Nature Microbiology, 7(10), 1547–1557. https:// doi.org/10.1038/s41564-022-01209-6
- Ravi, K., García-Hidalgo, J., Gorwa-Grauslund, M. F., & Lidén, G. (2017). Conversion of lignin model compounds by Pseudomonas putida KT2440 and isolates from compost. Applied Microbiology and Biotechnology, 101(12), 5059–5070. https://doi.org/10.1007/s00253-017-8211-y
- Recupido, F., Toscano, G., Tatè, R., Petala, M., Caserta, S., Karapantsios, T. D., & Guido, S. (2020). The role of flow in bacterial biofilm morphology and wetting properties. *Colloids and Surfaces*, *B: Biointerfaces*, 192, 111047. https://doi.org/10.1016/j.colsurfb.2020.111047
- Risse-Buhl, U., Anlanger, C., Kalla, K., Neu, T. R., Noss, C., Lorke, A., & Weitere, M. (2017). The role of hydrodynamics in shaping the composition and architecture of epilithic biofilms in fluvial ecosystems. Water Research, 127, 211–222. https://doi.org/10.1016/j.watres.2017.09.054
- Roosjen, A., Boks, N. P., van der Mei, H. C., Busscher, H. J., & Norde, W. (2005). Influence of shear on microbial adhesion to PEO-brushes and glass by convective-diffusion and sedimentation in a parallel plate flow chamber. *Colloids and Surfaces, B: Biointerfaces, 46*(1), 1–6. https://doi.org/10.1016/j.colsurfb.2005.08.009
- Rożej, A., Cydzik-Kwiatkowska, A., Kowalska, B., & Kowalski, D. (2015). Structure and microbial diversity of biofilms on different pipe

- materials of a model drinking water distribution systems. *World Journal of Microbiology and Biotechnology*, 31, 37–47. https://doi.org/10.1007/s11274-014-1761-6
- Samanta, S. K., Singh, O. V., & Jain, R. K. (2002). Polycyclic aromatic hydrocarbons: Environmental pollution and bioremediation. *Trends in Biotechnology*, 20(6), 243–248. https://doi.org/10.1016/S0167-7799(02)01943-1
- Sanfilippo, J. E., Lorestani, A., Koch, M. D., Bratton, B. P., Siryaporn, A., Stone, H. A., & Gitai, Z. (2019). Microfluidic-based transcriptomics reveal force-independent bacterial rheosensing. *Nature Microbiology*, 4(8), 1274–1281. https://doi.org/10.1038/s41564-019-0455-0
- Schulze, A., Mitterer, F., Pombo, J. P., & Schild, S. (2021). Biofilms by bacterial human pathogens: Clinical relevance-development, composition and regulation-therapeutical strategies. *Microbial Cell*, 8(2), 28–56. https://doi.org/10.15698/mic2021.02.741
- September, S. M., Els, F. A., Venter, S. N., & Brözel, V. S. (2007). Prevalence of bacterial pathogens in biofilms of drinking water distribution systems. *Journal of Water and Health*, 5(2), 219–227. https://doi.org/10.2166/wh.2007.004b
- Shen, Y., Huang, C., Monroy, G. L., Janjaroen, D., Derlon, N., Lin, J., Espinosa-Marzal, R., Morgenroth, E., Boppart, S. A., Ashbolt, N. J., Liu, W. T., & Nguyen, T. H. (2016). Response of simulated drinking water biofilm mechanical and structural properties to long-term disinfectant exposure. *Environmental Science & Technology*, 50(4), 1779–1787. https://doi.org/10.1021/acs.est.5b04653
- Stoodley, P., Dodds, I., Boyle, J. D., & Lappin Scott, H. M. (1998). Influence of hydrodynamics and nutrients on biofilm structure. *Journal of Applied Microbiology*, 85(S1), 195–28S. https://doi.org/10.1111/j. 1365-2672.1998.tb05279.x
- Suarez, C., Piculell, M., Modin, O., Langenheder, S., Persson, F., & Hermansson, M. (2019). Thickness determines microbial community structure and function in nitrifying biofilms via deterministic assembly. Scientific Reports, 9(1), 5110. https://doi.org/10.1038/ s41598-019-41542-1
- Sutera, S. P., & Skalak, R. (1993). The history of Poiseuille's law. Annual Review of Fluid Mechanics, 25(1), 1-20.
- Thomen, P., Robert, J., Monmeyran, A., Bitbol, A. F., Douarche, C., & Henry, N. (2017). Bacterial biofilm under flow: First a physical struggle to stay, then a matter of breathing. *PLoS One*, 12(4), e0175197. https://doi.org/10.1371/journal.pone.0175197
- Tlili, A., Corcoll, N., Arrhenius, Å., Backhaus, T., Hollender, J., Creusot, N., Wagner, B., & Behra, R. (2020). Tolerance patterns in stream biofilms link complex chemical pollution to ecological impacts. *Environmental Science & Technology*, 54(17), 10745–10753. https://doi.org/10.1021/acs.est.0c02975
- Torresi, E., Fowler, S. J., Polesel, F., Bester, K., Andersen, H. R., Smets, B. F., Plósz, B. G., & Christensson, M. (2016). Biofilm thickness influences biodiversity in nitrifying MBBRs-Implications on micropollutant removal. *Environmental Science & Technology*, 50(17), 9279–9288. https://doi.org/10.1021/acs.est.6b02007
- Trejo, M., Douarche, C., Bailleux, V., Poulard, C., Mariot, S., Regeard, C., & Raspaud, E. (2013). Elasticity and wrinkled morphology of *Bacillus subtilis* pellicles. *Proceedings of the National Academy of Sciences United States of America*, 110(6), 2011–2016. https://doi.org/10.1073/pnas.1217178110
- Vasudevan, R. (2014). Biofilms: Microbial cities of scientific significance. *Journal of Microbiology Experimentation*, 1(3), 14. https://doi.org/10.15406/jmen.2014.01.00014

- Ximenes, E., Hoagland, L., Ku, S., Li, X., & Ladisch, M. (2017). Human pathogens in plant biofilms: Formation, physiology, and detection. *Biotechnology and Bioengineering*, 114(7), 1403–1418. https://doi.org/10.1002/bit.26247
- Xu, L. C., Vadillo-Rodriguez, V., & Logan, B. E. (2005). Residence time, loading force, pH, and ionic strength affect adhesion forces between colloids and biopolymer-coated surfaces. *Langmuir*, 21(16), 7491–7500. https://doi.org/10.1021/la0509091
- Xu, R., Zhang, K., Liu, P., Han, H., Zhao, S., Kakade, A., Khan, A., Du, D., & Li, X. (2018). Lignin depolymerization and utilization by bacteria. *Bioresource Technology*, 269, 557–566. https://doi.org/10.1016/j.biortech.2018.08.118
- Yan, X., Lin, T., Wang, X., Zhang, S., & Zhou, K. (2022). Effects of pipe materials on the characteristic recognition, disinfection byproduct formation, and toxicity risk of pipe wall biofilms during chlorination in water supply pipelines. Water Research, 210, 117980. https://doi. org/10.1016/j.watres.2021.117980
- Yang, J. Q., Zhang, X., Bourg, I. C., & Stone, H. A. (2021). 4D imaging reveals mechanisms of clay-carbon protection and release. *Nature Communications*, 12(1), 622. https://doi.org/10.1038/s41467-020-20798-6
- Yoda, I., Koseki, H., Tomita, M., Shida, T., Horiuchi, H., Sakoda, H., & Osaki, M. (2014). Effect of surface roughness of biomaterials on *Staphylococcus epidermidis* adhesion. *BMC Microbiology*, 14(1), 234. https://doi.org/10.1186/s12866-014-0234-2
- Zhang, W., Sileika, T. S., Chen, C., Liu, Y., Lee, J., & Packman, A. I. (2011). A novel planar flow cell for studies of biofilm heterogeneity and flow-biofilm interactions. *Biotechnology and Bioengineering*, 108(11), 2571–2582. https://doi.org/10.1002/bit.23234
- Zhang, Y., Silva, D. M., Young, P., Traini, D., Li, M., Ong, H. X., & Cheng, S. (2022). Understanding the effects of aerodynamic and hydrodynamic shear forces on *Pseudomonas aeruginosa* biofilm growth. *Biotechnology and Bioengineering*, 119(6), 1483–1497. https://doi.org/10.1002/bit.28077
- Zheng, S., Bawazir, M., Dhall, A., Kim, H. E., He, L., Heo, J., & Hwang, G. (2021). Implication of surface properties, bacterial motility, and hydrodynamic conditions on bacterial surface sensing and their initial adhesion. Frontiers in Bioengineering and Biotechnology, 9, 82. https://doi.org/10.3389/fbioe.2021.643722
- Zhu, I. X., Getting, T., & Bruce, D. (2010). Review of biologically active filters in drinking water applications. *Journal-American Water Works Association*, 102(12), 67–77. https://doi.org/10.1002/j.1551-8833. 2010.tb11364.x

SUPPORTING INFORMATION

Additional supporting information can be found online in the Supporting Information section at the end of this article.

How to cite this article: Wei, G., & Yang, J. Q. (2023). Impacts of hydrodynamic conditions and microscale surface roughness on the critical shear stress to develop and thickness of early-stage *Pseudomonas putida* biofilms. *Biotechnology and Bioengineering*, 1–12. https://doi.org/10.1002/bit.28409